NDH complex-mediated cyclic electron flow in bundle sheath cells enables C_4 photosynthesis

Maria Ermakova[1,2]*, Russell Woodford[1], Duncan Fitzpatrick[1], Soraya M. Zwahlen[1], Graham Farquhar[1], Susanne von Caemmerer[1], Robert T. Furbank[1]

[1] Centre of Excellence for Translational Photosynthesis, Division of Plant Science, Research School of Biology, Australian National University, Acton, ACT, Australia.

[2] School of Biological Sciences, Monash University, Melbourne, Victoria 3800, Australia.

*Correspondence to maria.ermakova@monash.edu.

Maria Ermakova, maria.ermakova@monash.edu, ORCID: 0000-0001-8466-4186

Russell Woodford, Russell.Woodford@anu.edu.au, ORCID: 0000-0002-6766-2274

Duncan Fitzpatrick, fitzpatrick.duncan@gmail.com

Soraya M. Zwahlen, u6355224@alumni.anu.edu.au, ORCID: 0000-0003-2130-3820

Graham Farquhar, graham.farquhar@anu.edu.au

Susanne von Caemmerer, Susanne.Caemmerer@anu.edu.au, ORCID: 0000-0002-8366-2071

Robert Furbank, robert.furbank@anu.edu.au, ORCID: 0000-0001-8700-6613

ME, RF and SvC designed the research; RF, SvC and GF obtained funding; ME generated gene-edited plants; ME, RW, DF and SZ performed research; ME, RW and DF analysed data; ME, RW and RF wrote the paper; all authors discussed the results and contributed to the final manuscript.

Abstract

The superior productivity of C_4 plants is achieved via a metabolic C_4 cycle which acts as a CO_2 pump across mesophyll and bundle sheath (BS) cells and requires an additional input of energy in the form of ATP. Chloroplast NADH dehydrogenase-like complex (NDH) increases ATP production in C_3 plants by operating cyclic electron flow (CEF) around Photosystem I (PSI), and its importance for C_4 photosynthesis has been proposed from evolutionary and reverse genetics studies. We used the gene-edited C_4 species *Setaria viridis* with null *ndhO* alleles lacking NDH to study a contribution of the complex to the cell-level electron transport. Our results indicate that NDH is the primary PSI electron acceptor mediating the majority of CEF in BS cells whilst the

contribution of the complex to CEF in mesophyll cells is minimal. Moreover, the reduced leaf CO_2 assimilation rate and growth of plants lacking the complex cannot be rescued by supplying additional CO_2, indicating that NDH is essential for generating ATP required for CO_2 fixation by the C_3 cycle. Hereby we resolve a cell-level mechanism for the contribution of NDH to supporting high CO_2 assimilation rates in C_4 photosynthesis.

Introduction

C_4 plants typically exhibit superior radiation, water and nitrogen use efficiency allowing them to outperform C_3 plants in warm climates[1,2]. The C_4 cycle operates across mesophyll and bundle sheath (BS) cells as a biochemical carbon concentrating mechanism (Fig. 1). This increases CO_2 partial pressure in BS cells where Rubisco and other Calvin-Benson-Bassham cycle (hereafter, the C_3 cycle) enzymes reside[3]. The C_4 cycle begins in the mesophyll cytosol with the conversion of CO_2 to HCO_3^- by carbonic anhydrase which is then fixed by PEP carboxylase (PEPC) into the C_4 acid oxaloacetate. The latter can be reduced to malate or transaminated to aspartate before diffusing to BS cells for decarboxylation. There are three major subtypes of C_4 photosynthesis, categorised by the primary decarboxylating enzyme[4]. As the majority of agriculturally important C_4 species such as maize, sugarcane, sorghum and millets, use $NADP^+$-dependent malic enzyme (NADP-ME) to decarboxylate malate in BS chloroplasts, this subtype is the major focus of C_4 photosynthesis research and of this study. Decarboxylation of malate releases CO_2, reduces $NADP^+$ to NADPH and produces pyruvate which returns to mesophyll cells and is regenerated into PEP to complete the C_4 cycle. Engineering C_3 plants to carry out C_4 photosynthesis is considered a promising route to increasing crop productivity, prompting attempts to introduce the C_4 pathway into the C_3 plant rice[5,6]. However, these projects are hampered by our incomplete understanding of the molecular mechanisms of C_4 photosynthesis. Electron transport reactions crucial for providing at least two extra ATP molecules for each CO_2 fixed – the additional energy cost of the carbon concentrating mechanism — is one such mechanism we aim to address in this work.

In the C_4 system, the electron transport chains of mesophyll and BS cells are tailored for specific metabolic needs[7] (Fig. 1). The mesophyll electron transport chain closely resembles that of C_3 plants, where linear electron flow (LEF) from Photosystem II (PSII) to Photosystem I (PSI) results in production of NADPH. Cytochrome b_6f complex (Cytb_6f) between the two photosystems couples electron transport with proton translocation across the thylakoid membrane, which establishes a proton motive force (*pmf*) used by ATP synthase to generate ATP. For the C_4 cycle, NADPH produced in mesophyll cells is primarily used for reducing oxaloacetate to malate while the ATP produced here is used to regenerate PEP; both are also used for the generation of triose phosphate within the C_3 cycle (see below). The ΔpH component of *pmf* is also a key signal controlling electron transport rate by (i) slowing down Cytb_6f activity to restrict electron flow to PSI, also known as 'photosynthetic control'[8], and (ii) initiating a dissipation of absorbed light energy as heat through the rapidly-formed and reversible form of non-photochemical quenching (NPQ)[9]. This form of NPQ is activated by protonating lumen-exposed residues of the PsbS protein[10] and through the conversion of violaxanthin to zeaxanthin in the antennae[11].

65 LEF alone is often unable to satisfy the combined ATP/NADPH requirements of photosynthesis and other
66 metabolic processes[12]. The C_3 cycle in BS cells needs 3 mols of ATP and 2 mols of NADPH to fix 1 mol of CO_2.
67 While malate decarboxylation provides at least half of the required NADPH, mesophyll electron transport also
68 supplies NADPH and ATP through the triose phosphate shuttle in which a part of the 3-PGA produced by
69 Rubisco diffuses to the mesophyll cells for conversion to triose phosphate, which then returns to the BS[3,13] (Fig.
70 1). This results in a lower requirement to produce NADPH in BS cells in which abundance and activity of PSII
71 are diminished compared to the mesophyll[14]. It has long been proposed that to predominantly yield ATP, BS
72 cells maintain active cyclic electron flow (CEF) that returns electrons from the reducing side of PSI back to the
73 plastoquinone pool, allowing electrons to again pass through Cytb_6f and increase *pmf*[15,16]. There are two major
74 proposed CEF pathways: via PROTON GRADIENT REGULATION5 (PGR5) and via the chloroplast NADH
75 dehydrogenase-like complex (NDH)[17]. Abundance of both PGR5 and NDH in leaves increased during the
76 evolutionary transition from C_3 to C_4 plants[18,19] and NDH subunits preferentially accumulated in BS cells[20-22]. In
77 C_3 plants, NDH comprises only 0.2% of total thylakoid protein content[23] and mutants lacking the complex retain
78 normal fitness under optimal growth conditions[24]. In contrast, lowering NDH content in C_4 species maize and
79 *Flaveria bidentis* had severe effects on photosynthesis and growth[25-27]. While a direct mechanism for this effect
80 has not been resolved, these observations prompted suggestions that NDH is involved in ATP production via
81 CEF[26] required for concentrating CO_2 in BS cells[25]. Here we use CRISPR/Cas9 in a model C_4 plant of NADP-ME
82 subtype *Setaria viridis* to create plants lacking NDH and provide the first functional demonstration of NDH
83 activity in C_4 BS cells.

84 ## Results

85 **Creating *S. viridis* plants with null *ndhO* alleles**

86 To create null *ndhO* alleles, known to result in the arrested assembly of NDH[25], we targeted Cas9 to the third
87 and the fifth exons of *S. viridis ndhO* (Fig. 2a). Two new *ndhO* alleles were obtained: *ndhO-2* with a single
88 nucleotide insertion causing a frameshift mutation, resulting in an altered amino acid (aa) sequence starting
89 from S23 and a premature termination codon, and *ndhO-6* with a single nucleotide deletion causing a
90 frameshift mutation, resulting in an altered aa sequence starting from G67 (Fig. S1). *S. viridis* plants with
91 homozygous *ndhO-2* and *ndhO-6* alleles (*ndh* hereafter) lacked NDH as confirmed by immunoblotting of leaf
92 extracts with antibodies against the NdhH subunit of the complex (Fig. 2b). In the absence of NDH, plants
93 showed severe reduction of the aboveground biomass to about 30% of wild type (WT, Fig. 2d), which could
94 not be rescued by supplementing air in the growth room with 2% CO_2, a treatment previously shown to
95 improve growth of *S. viridis* deficient in carbon concentrating mechanism[28,29]. The CO_2 response of CO_2
96 assimilation rate in *S. viridis ndh* plants closely resembled the maize *ndhO* mutant[25], with assimilation reduced
97 to about 50% of WT-level at intercellular CO_2 partial pressures above 100 µbar (Fig. 2e). No differences
98 between *ndhO-2* and *ndhO-6* plants indicated that both edited alleles resulted in inactive NDH.

99 **Content of chlorophyll and photosynthetic proteins**

100 Leaf contents of metabolic enzymes, PEPC, the large subunit of Rubisco (RbcL) and sedoheptulose-
101 bisphosphatase (SBPase) of the C_3 cycle, were unaltered in *ndh* plants (Fig. 2b, Fig, S2a). Relative abundances
102 of some electron transport components, the D1 subunit of PSII, the AtpB subunit of ATP synthase and PsbS,
103 did not differ between the gene-edited and WT plants per leaf area. However, plants lacking NDH had
104 significantly less of the Rieske subunit of Cytb_6f, the PsaB subunit of PSI and PGR5 per leaf area, compared to
105 WT (Fig. S2b). The total leaf Chl content was about 30% lower in *ndh* plants (Table S1). Mesophyll Chl content
106 per leaf area was also significantly decreased in plants lacking NDH, whilst the BS Chl content was unaltered,
107 compared to WT (Table S1).

108 The overall composition of thylakoid membranes was largely unaffected in mesophyll and BS cells of *ndh*
109 plants, compared to WT (Fig. S2c), but cell-level changes in abundances of some electron transport
110 components were detected by immunoblotting (Fig. 3). NDH complex was predominantly found in BS cells of
111 WT plants. Relative contents of AtpB, PGR5 and PsbS per Chl were increased in BS cells of *ndh* plants (Fig. 3b)
112 whilst Rieske and PGR5 abundance was significantly decreased in mesophyll cells of *ndhO* plants, compared to
113 corresponding WT cells.

114 **Electron fluxes in bundle sheath cells**

115 Effects of the lack of NDH on BS electron transport were examined by membrane inlet O_2 mass spectrometry
116 and spectroscopy using isolated BS strands supplied with $NaHCO_3$ and triose phosphate to support
117 CO_2 assimilation[30]. The rate of gross O_2 evolution by PSII in *ndh* BS cells was double that of the WT BS (P =
118 0.037, Fig. 4a). Next, electron flux through PSI was compared by monitoring the absorbance signal of $P700^+$, a
119 cation of the reaction centre of PSI. The maximum oxidisable P700, P_M, was similar between *ndhO* and WT
120 plants (P = 0.55) indicating a similar amount of active PSI (Fig. 4b). These measured PSII and PSI activities were
121 in line with relative abundances of D1 and PsaB in BS cells (Fig. 3).

122 The $P700^+$ signal was next monitored from BS cells adapted to actinic light of 1000 µmol m^{-2} s^{-1} upon the
123 application of strong far-red light and a saturating pulse allowing estimation of the photochemical yield of PSI
124 (ϕ_I) and the non-photochemical yields of the acceptor (ϕ_{NA}) and donor (ϕ_{ND}) sides of PSI (Fig. 4c). The traces
125 were normalised at the minimal level of $P700^+$ after a dark relaxation, and the steady-state (P) and maximum
126 (P_M') levels of P700 oxidation under light were determined as shown in Fig. 4c. The addition of malate
127 drastically reduced ϕ_{NA}, *i.e.*, the loss of PSI activity due to a lack of acceptors, in WT BS cells (P = 0.00003),
128 compared to the value without malate (Fig. 4d). Concurrently, the addition of malate increased ϕ_I (by about
129 50%, P = 0.001) and ϕ_{ND} (*i.e.*, the loss of PSI activity due to a lack of electrons on the donor side, P = 0.0003) in
130 WT BS cells, compared to values without malate (Fig. 4e,f). BS cells of *ndh* plants showed 36% lower ϕ_I (P =
131 0.041) as well as higher ϕ_{NA} (P = 0.001) and lower ϕ_{ND} (P = 0.003) compared to WT BS cells already in the
132 absence of malate. The addition of malate did not result in any significant changes in PSI activity in *ndh* BS cells
133 (P = 0.99 for ϕ_I, 0.16 for ϕ_{NA} and 0.12 for ϕ_{ND}). Consequently, in the presence of malate, ϕ_I and ϕ_{ND} were about

134 50% lower than in WT BS cells (P = 0.00003 and P = 0.0001 respectively) while ϕ_{NA} was 4-fold higher (P =
135 0.000004) in *ndh* BS cells compared to WT.

136 The initial decay of $P700^+$ signal upon the termination of actinic light provides an estimate of a relative rate of
137 P700 re-reduction from the intersystem electron transport chain (Fig. 4g,h). Despite a WT-like Cytb_6f content
138 (Fig. 3), *ndh* showed about 40% slower PSI reduction than WT plants in the absence of malate (P = 0.0128). The
139 addition of malate accelerated the reduction of PSI in WT BS cells (P = 0.0158) but not in *ndh* BS cells (P = 0.92),
140 compared to the rate without malate, resulting in about 50% lower reduction rate in the mutant compared to
141 WT (P = 0.0003). The addition of methyl viologen (MV, a strong electron acceptor competing for electrons from
142 PSI with CEF) together with malate allowed estimating the rate of P700 re-reduction by LEF only (Fig. 4g,h). In
143 the presence of MV, the PSI reduction rate in BS cells was drastically reduced to about 16% and 13% in WT and
144 *ndh*, respectively, compared to the rates observed with malate only.

145 **Leaf photosynthesis**

146 Absence of NDH had significant impact on leaf electron transport and gas-exchange properties. Although the
147 maximum photochemical efficiency of PSII (F_V/F_M) did not differ between the genotypes (Table S1), in *ndh*
148 plants up to 50% less light absorbed by PSII was used for photochemical reactions (ϕ_{II}) at all irradiances (Fig.
149 5a). The yield of regulated non-photochemical reactions (ϕ_{NPQ}) was increased up to 2-fold in *ndh* leaves below
150 1600 µmol m^{-2} s^{-1}, whilst the non-regulated non-photochemical yield (ϕ_{NO}) was mostly unaltered, compared to
151 WT (Fig. 5b and Fig. 5c). Due to the low PSII content in BS cells (Fig. 3), leaf chlorophyll a fluorescence originates
152 mostly from mesophyll cells, whereas leaf $P700^+$ absorbance reports on PSI activity in both mesophyll and BS
153 cells. Plants lacking NDH had on average lower ϕ_I which was significantly reduced to about 50% of WT level at
154 irradiances above 1500 µmol m^{-2} s^{-1} (Fig. 5d). The non-photochemical yields of PSI showed contrasting
155 responses depending on irradiance. Below 200 µmol m^{-2} s^{-1}, the loss of PSI photochemical efficiency in *ndh* was
156 due to a lack of electron supply on the donor side whilst above 400 µmol m^{-2} s^{-1} it was due to the lack of
157 acceptors (Fig. 5e and Fig. 5f).

158 Plants lacking NDH exhibited about 50% lower CO_2 assimilation rates at all irradiances (Fig. 5g) and lower
159 quantum yield of CO_2 assimilation, compared to WT (Table S1). The ratio of intercellular to ambient CO_2 partial
160 pressures (C_i/C_a), was significantly higher in *ndh* plants at all irradiances (Fig. 5h), compared to WT, indicating
161 a higher CO_2 availability at the site of primary carboxylation (*i.e.*, in the cytosol of mesophyll cells). Calculated
162 relative electron flux through PSII was significantly lower at all irradiances (Fig. 5i) whilst the slope of the
163 relationship between NPQ and electron flux was drastically increased (Fig. S3) in plants lacking NDH in
164 comparison to WT.

165 **Proton fluxes in mesophyll cells**

166 Since no changes in electrochromic shift signal could be detected from the dark-adapted isolated BS cells in
167 response to a saturating flash (Fig. S4a), leaf electrochromic shift signal was reported on thylakoid membrane
168 energisation in mesophyll cells. Total *pmf*, which represents a balance between a build-up and dissipation of a

169 transmembrane proton gradient, was similar between *ndh* and WT plants below 300 µmol m^{-2} s^{-1} and
170 significantly decreased in the gene-edited plants at higher irradiances (Fig. 6a). Proton conductivity of the
171 thylakoid membrane (g_{H+}), indicative of the flux through ATP synthase, was significantly decreased in *ndh*
172 leaves at 50 µmol m^{-2} s^{-1} but similar to WT at irradiances above that (Fig. 6b). The relationship between the
173 light-driven proton flux through the thylakoid membrane (ν_{H+}) and the relative electron flux through PSII (i x
174 ϕ_{II}), indicative of the CEF/LEF ratio[31], remained constant between *ndh* and WT plants (Fig. 6c). However, the
175 relationship between NPQ and *pmf* was markedly altered so that in *ndh* plants, for a given *pmf*, NPQ was
176 approximately 2-fold higher than in WT (Fig. 6d). This altered relationship was not caused by changes in
177 partitioning between ΔpH and Δψ (Fig. S4c and Fig. S4d). Moreover, a build-up of NPQ occurred at a similar
178 rate upon illumination and, at 1 min after the termination of illumination, NPQ relaxed to a similar level in *ndh*
179 and WT plants (Fig. S5).

180 Discussion

181 NDH is believed to have evolved from the cyanobacterial NDH-1 complex[32] and is largely conserved in the
182 green lineages[33]. Despite being non-essential in normal conditions, due to its ability to maximise *pmf* during
183 CEF[34], NDH abundance increases in C_3 plants in response to elevated ATP demand[35] to facilitate plant
184 acclimation to low or fluctuating light[36,37]. During the evolutionary transition from C_3 to C_4 plants, NDH levels
185 increased concurrently with the emergence of C_4-like species coinciding with the appearance of the C_4 cycle as
186 a CO_2 pump[38]. Supporting an essential role of NDH in C_4 photosynthesis, generated here *S. viridis* plants lacking
187 NDH could not efficiently use absorbed light and reached only low assimilation rates (Fig. 2e and Fig. 5g).
188 However, in contrast to mutants and transgenic plants with an impaired carbon concentrating mechanism[28,29],
189 growth of *ndh* plants did not recover at high CO_2 (Fig. 2d). Therefore, NDH is not directly involved in the C_4
190 cycle or concentrating CO_2 in BS cells as previously proposed[25]; instead, our results indicate that NDH is
191 essential for supporting CO_2 assimilation by the C_3 cycle.

192 Active CEF in BS cells has long been proposed to increase the ATP yield of C_4 plants and contribute to fulfilling
193 the energy demand of the carbon concentrating mechanism[15,39]. The measured CEF to LEF ratio (CEF/LEF) of
194 C_4 leaves of about 1.7 greatly exceeded the C_3 leaf value of 0.9[40] but no experimental estimates of CEF in BS
195 cells were available. To study BS electron transport properties, here we isolated BS strands from leaves of *S.*
196 *viridis* and supplied all preparations with triose phosphate and $NaHCO_3$ to satisfy NADPH and (partially) CO_2
197 requirements of the C_3 cycle[30]. Thus, the electron transport chain of BS cells only needed to produce ATP to
198 support C_3 cycle activity. A strong ϕ_{NA} in WT BS cells in the absence of malate and its drastic decrease
199 (combined with an increase of ϕ_{ND}) after the malate addition corroborated that, without malate, activity of the
200 C_3 cycle was limited by CO_2 availability and potentially also by NADPH. CO_2 and NADPH derived from malate
201 increased the demand of the C_3 cycle for ATP which doubled PSI activity in WT BS cells (Fig. 4e). In those
202 conditions, 86% of electrons reducing PSI belonged to CEF (Fig. 4h), producing a CEF/LEF ratio of >6 which
203 closely resembled the model predictions[41]. These results provided long forthcoming experimental evidence for
204 PSI driving active CEF in C_4 BS cells set to supply ATP for the C_3 cycle.

205 Detailed electron transport analysis of BS cells from *ndh* plants showed that NDH mediated a large portion of
206 CEF and was the primary electron acceptor from PSI in BS cells. These conclusions were supported by a
207 decreased PSI reduction capacity (Fig. 4h) and a strong PSI acceptor side limitation observed in BS cells of *ndh*
208 plants (Fig. 4d). A 50% lower PSI activity in BS cells in the absence of NDH was proportional to the reduction of
209 leaf CO_2 assimilation rate (Fig. 2e and Fig. 5g) demonstrating the indispensable role of NDH-CEF in BS ATP
210 production. Interestingly, even in the absence of NDH, most of the electrons reducing PSI belonged to CEF (Fig.
211 4h). This residual CEF could be linked to PGR5, as suggested by the increased PGR5 content in BS cells of *ndh*
212 plants (Fig. 3a), and/or to other unknown CEF pathways. Molecular mechanisms of PGR5's action are, however,
213 still under debate[42], and further investigation is required to determine whether it contributes to ATP
214 production in BS cells or is mainly involved in photoprotection[27,43]. It is also worth mentioning that electron
215 transport limitations detected in BS cells of *ndh* plants were unlikely to be caused by photosynthetic control.
216 Since BS cells have low LEF (Fig. 4a,h), the C_3 cycle is not the primary PSI electron acceptor and does not
217 regulate PSI activity through NADPH consumption. Therefore, PSI (and hence CEF) activity in BS cells is likely
218 regulated via photosynthetic control that restricts electron transport at Cytb_6f to match the capacity of CO_2
219 assimilation reactions. In BS cells of *ndh* plants, electron transport was limited even in the presence of malate
220 despite an apparent easing up of photosynthetic control observed in WT BS cells upon malate addition (Fig. 4)
221 due to increased ATP demand upon providing CO_2 and NADPH.

222 Alternatively, a lack of PSI stimulation in response to malate in BS cells of *ndh* plants could also be explained
223 by inefficient malate decarboxylation *in vivo*. A supply of triose phosphate combined with an impaired ATP
224 generation capacity of BS cells in the absence of NDH likely resulted in an elevated $NADPH/NADP^+$ ratio and
225 unavailability of $NADP^+$ for malic enzyme. This could indicate a potential function of NDH in facilitating NADPH
226 oxidation and using electrons derived from it for poising CEF. In C_3 mesophyll chloroplasts, a respiration-like
227 non-photochemical reduction of the PQ pool from stromal reductants by NDH is a part of the chlororespiratory
228 pathway dissipating energy together with the plastidial terminal oxidase[44]. In C_4 plants, electron donation from
229 stromal donors to CEF is supported by observations of malate-driven carbon reduction in sorghum BS cells
230 independent of PSII activity[45] and by the capacity for reduction of PSI following malate addition to maize BS
231 cells[46]. Since BS cells are effectively constantly light-limited due to shading by mesophyll[41,47], driving CEF with
232 minimal PSII engagement would maximise the light received by PSI potentially contributing to the observation
233 that the highest quantum yields across all C_4 decarboxylation types are seen in plants utilizing the NADP-ME
234 photosynthetic mechanism[48]. However, the reverse reaction of the plant chloroplast ferredoxin:$NADP^+$
235 oxidoreductase (FNR, Fig. 1), also required for reduction of the PQ pool from stromal NADPH, although
236 theoretically possible and utilised *in vitro*[49], is yet to be shown *in vivo*.

237 The mesophyll CEF/LEF ratio was not affected in *ndh* plants (Fig. 6c), which was comparable to the low impact
238 of NDH deletion on CEF in C_3 plants in optimal conditions[35]. Instead, lower mesophyll Chl content (Table S1),
239 lower electron flux through PSII and higher NPQ (Fig. 5, Fig. S3) in *ndh* plants resembled effects observed in
240 *Flaveria bidentis* with genetically reduced Rubisco abundance[50]. This observation suggested that the absence

241 of NDH in the BS and inability of the C_3 cycle to efficiently assimilate CO_2 provided a negative feedback on the
242 C_4 cycle resulting in downregulation of mesophyll electron transport. Interestingly, since *pmf* in *ndh* plants was
243 significantly lower than in WT at irradiances above 500 µmol m^{-2} s^{-1} (Fig. 6), there was an increased sensitivity
244 of NPQ to *pmf* (Fig. 6d). An altered relationship between NPQ and ΔpH (or *pmf*) has been previously reported
245 in some genetically modified plants, for instance, lacking or over-producing chloroplast NADPH-dependent
246 thioredoxin reductase, or with increased Cytb_6f abundance[51,52]. These alterations are likely a result of
247 perturbed stromal redox regulation and are mediated through the chloroplast thioredoxin system which
248 directly targets multiple NPQ components[52,53]. The increased sensitivity of NPQ in *ndh* plants was therefore
249 also in line with persistent mesophyll stroma overreduction due to accumulation of NADPH caused by a slow-
250 down of the C_4 cycle activity in response to C_3 cycle limitation.

251 **Conclusion**

252 In NADP-ME species, NADPH for the C_3 cycle can be supplied from mesophyll cells through the influx of malate
253 and triose phosphate whilst providing ATP for regeneration of ribulose 1,5-bisphosphate, the substrate of
254 Rubisco, is required in the BS (Fig. 1). The BS electron transport chain therefore becomes specialised to
255 primarily generate ATP by operating active CEF. Impaired CEF in the absence of NDH jeopardises the supply of
256 ATP to the C_3 cycle, thus, making NDH indispensable for C_4 photosynthesis. Engineering a fully operational
257 NADP-ME type C_4 photosynthesis into C_3 plants will require upregulating NDH abundance in BS cells to achieve
258 the desired increases in assimilation and radiation use efficiency.

259 **Materials and Methods**

260 **Construct assembly, transformation and selection of edited plants**

261 *S. viridis* plants with null *ndhO* alleles were created using CRISPR/Cas9 gene-editing. The genomic and coding
262 sequences of *S. viridis ndhO* (Sevir.5G467100) were obtained from Phytozome (https://phytozome-
263 next.jgi.doe.gov). Two 19 nt gRNAs fitting the search criteria 'A..19N..NGG' within an exon, where NGG is the
264 protospacer adjacent motif, were selected using CRISPOR[54] (Fig. 2a). The use of 'A' for the first base of gRNAs
265 was required to maximise the expression from *Oryza sativa* snoRNA *U3* (*OsU3*) promoter[55]. The *cas9* gene and
266 *OsU3* promoter sequences were obtained from pRGEB32[56] (Addgene) and adapted for the Golden Gate cloning
267 system[57]. To create a gene construct for *ndhO* editing (Fig. 2b), the first expression module in a plant binary
268 vector pAGM4723 was occupied by the hygromycin phosphotransferase gene (*hpt*) driven by the *O. sativa*
269 *Actin1* (*OsAct1*) promoter. The second expression module contained *cas9* under the control of *Z. mays*
270 *Ubiquitine1* (*ZmUbi1*) promoter. Both *hpt* and *cas9* were supplied with the bacterial nopaline synthase
271 terminator. The third expression module in pAGM4723 was occupied by the two selected gRNAs forming a
272 single synthetic polycistronic gene, assembled according to Xie, et al. [56], to be processed via the endogenous
273 tRNA-processing system, under the control of *OsU3* promoter. The resulting construct was transformed into
274 *S. viridis* cv. MEO V34-1 using the *Agrobacterium tumefaciens* strain AGL1[58]. T_0 plants resistant to hygromycin
275 were transferred to soil and analysed for *hpt* copy number by digital PCR (iDNA Genetics, Norwich, UK).

276 To select T_0 plants with active Cas9, DNA was extracted from leaves with the DNeasy Plant kit (Qiagen, Venlo,
277 The Netherlands) and the region of *ndhO* spanning both gRNAs was amplified using the primers
278 CGCGTGGACAAGGAGAAGTA and CGTAGTCCAGCTTGTCCGAC. PCR products were sequenced and the edited
279 *ndhO* alleles identified using Geneious Prime (https://www.geneious.com). Selected T_0 plants were self-
280 pollinated and their progeny analysed by digital PCR to retain only the plants that segregated out the T-DNA.
281 Next, *ndhO* was sequenced to select the plants homozygous for *ndhO-2* and *ndhO-6* alleles (Fig. S1). The T_2
282 progenies of those homozygous plants were used in all subsequent experiments. Gene and protein sequences
283 were visualised in Geneious Prime, and protein structures were modelled using AlphaFold2[59] and Mol*[60].

284 **Plant growth conditions**

285 All plants were grown in a controlled environment room with a 16 h light/8 h dark photoperiod, 28°C day, 22°C
286 night, 60% humidity and ambient CO_2 (if not stated otherwise) at a light intensity of 300 µmol m^{-2} s^{-1} supplied
287 by 1000 W red sunrise 3200K lamps (Sunmaster Growlamps, Solon, OH). For the high CO_2 growth experiment,
288 air in the growth room was supplied with 2% CO_2. For plants grown from seeds, seeds were surface-sterilised
289 in 10% bleach and germinated on a rooting medium (pH 5.7) containing 2.15 g L^{-1} Murashige and Skoog salts,
290 10 ml L^{-1} 100× Murashige and Skoog vitamins stock, 30 g L^{-1} sucrose and 7 g L^{-1} Phytoblend. Seedlings that
291 developed secondary roots were transferred to 0.6 L pots with garden soil mix layered on top with 2 cm of
292 seed raising mix (Debco, Tyabb, Australia) both containing 1 g L^{-1} Osmocote (Scotts, Bella Vista, Australia).
293 Wild-type (WT) *S. viridis* plants were used as control in all experiments. Youngest fully expanded leaves of the
294 3–4-week-old plants, before flowering, were used for all analyses.

295 **Chl analysis**

296 Chl content in leaves, bundle sheath strands and protein samples was measured in 80% acetone buffered with
297 25 mM HEPES-KOH (pH 7.8) according to Porra, et al. [61]. The portion of leaf Chl in BS cells (Chl_{BS} / Chl_{leaf}) was
298 calculated from the RbcL immunoblots as described in Ermakova, et al. [14]. Chl contents of BS and mesophyll
299 cells per leaf area (Chl_{BS} and Chl_{MES}, Table S1) were calculated by multiplying leaf Chl content by the portion of
300 leaf Chl in BS cells or in mesophyll.

301 **Blue-native PAGE, SDS-PAGE and immunoblotting**

302 Thylakoid isolation and Blue-native PAGE were performed as described in Ermakova, et al. [51]. For protein
303 analysis, BS strands were isolated following the procedure of Ghannoum, et al. [62]. Protein isolation from leaves
304 and BS strands, SDS-PAGE and immunoblotting were performed as described in Ermakova, et al. [14]. Aliquots
305 were taken from protein samples for Chl analysis immediately after grinding. Samples were loaded either on
306 leaf area or Chl (*a*+*b*) basis. Membranes were probed with antibodies against photosynthetic proteins: NdhH
307 (1:3000, AS164065, Agrisera, Vännäs, Sweden), RbcL (1:10,000,[63]), PEPC (1:10,000,[64]), SBPase (1:3000,
308 AS152873, Agrisera), D1 (1:10,000, AS10704, Agrisera), Rieske (1:5000, AS08330, Agrisera), PsaB (1:5000, AS10
309 695, Agrisera), AtpB (1:10,000, Agrisera), PGR5 (1:3000, AS163985, Agrisera, verification of this antibody is
310 shown in Fig. S6), PsbS (1:3000, AS09533, Agrisera), Lhcb2 (1:10,000, AS01003, Agrisera). Quantification of

311 immunoblots was performed with Image Lab software (Bio-Rad, Hercules, CA, USA). Relative protein
312 abundances per unit of Chl in leaves (P_{leaf}) and BS cells (P_{BS}) were estimated from the immunoblots (Fig. 3).
313 Using Chl contents of leaves and cells per leaf area (Chl_{leaf}, Chl_{BS} and Chl_{MES} in Table S1), relative protein
314 abundances per unit of Chl in mesophyll cells (P_{MES}) were calculated as described in Ermakova, et al. [14] assuming
315 that: $P_{leaf} \times Chl_{leaf} = P_{BS} \times Chl_{BS} + P_{MES} \times Chl_{MES}$.

316 **O_2 evolution of BS strands**

317 For activity assays, BS strands were isolated following the procedure of Furbank and Badger [30], resuspended in
318 activity buffer (10 mM HEPES-KOH, pH 7.4, 2 mM $MgCl_2$, 2 mM KH_2PO_4, 10 mM KCl, 0.3 M sorbitol) to a Chl
319 (*a* + *b*) concentration of 25 µg mL^{-1}, purged with N_2 gas and kept on ice. Membrane inlet mass spectrometry
320 (MIMS) was used to measure the steady-state gross O_2 evolution rates through the production of $^{16}O_2$ from
321 suspensions of BS cells at a saturating irradiance (1000 µmol m^{-2} s^{-1}). The system consisted of a magnetically
322 stirred, thermally controlled at 25 °C sample cuvette separated from the high vacuum line of a Thermo Delta
323 V ion ratio mass spectrometer (Thermo Electron Corp, Bremen, Germany) via a Teflon membrane (Hansatech
324 Instruments, Norfolk, UK). The top lid of the cuvette had a quartz window through which halogen light was
325 supplied through a fibre optic and a septum. BS suspensions were loaded into the cuvette, purged with N_2 and
326 then supplied with 1 mM HCO_3^-, 1 mg mL^{-1} carbonic anhydrase and 5 mM dihydroxyacetone phosphate to
327 support CO_2 assimilation[30]. Samples were left in darkness for 5 mins to reach equilibrium, followed by initiation
328 of data acquisition for 2.5 min in the dark and 5 min at 1000 µmol m^{-2} s^{-1}. Rates and calibrations were conducted
329 as described in Beckmann, et al. [65].

330 **P700 spectroscopy on BS strands**

331 For P700 measurements, 1 mL aliquot of BS suspension was incubated for five minutes at room temperature
332 with 100 mM $NaHCO_3$ and 5 mM dihydroxyacetone phosphate to support CO_2 assimilation[30] and with 10 mM
333 malate and 200 µM methyl viologen when required. The suspension was then filtered via gentle vacuum onto
334 a glass fiber disc (Whatman, Buckinghamshire, UK). The disc was saturated with activity buffer and metabolites
335 and loaded into the measurement cuvette set at 25 °C. Redox changes of P700 were measured using the
336 method and a set-up of Kou, et al. [66]. A dual wavelength (820/870 nm) unit ED-P700DW (Heinz Walz, Effeltrich,
337 Germany) was attached to a pulse amplitude modulation fluorometer PAM-101 (Heinz Walz) in the reflectance
338 mode. The signal was zeroed in darkness before measurements were made. To determine P_M, the maximal
339 $P700^+$ signal, samples without added malate were illuminated with weak far-red light of 30 µmol m^2 s^{-1} to
340 preferentially drive PSI photochemistry, over which a saturating pulse (10 µs at 9000 µmol m^2 s^{-1}) was
341 triggered.

342 Next, samples were illuminated for three minutes with white actinic light of 1000 µmol m^2 s^{-1} to reach a steady-
343 state. The same actinic light was then maintained for 9.016 s, using an electronic shutter controlled by one
344 terminal of a pulse/delay generator (Model 555, Berkeley Nucleonics, San Rafael, CA, USA). During the 9.016-
345 s illumination cycle, data acquisition (using software written by the late AB Hope) was started by a second

346 terminal of the pulse/delay generator yielding P, a steady-state $P700^+$ level. At 8.85 s, a strong far-red light
347 (2000 µmol m^{-2} s^{-1}) from an LED (741 nm ± 13 nm, LED735–66–60, Roithner LaserTechnik, Vienna, Austria) was
348 triggered on for 100 ms using a third terminal of the pulse/delay generator to help oxidise P700[50]. While the
349 far-red light was on, at 8.90 s, a saturating light pulse (9000 µmol m^{-2} s^{-1}) was applied for 20 ms from a fourth
350 terminal of the pulse/delay generator, yielding P_M', the maximal oxidised level of P700 under light. Finally, the
351 white actinic light was turned off by the electronic shutter at 9.016 s whilst the data acquisition continued for
352 85 ms. Immediately after a completion of one cycle of illumination and data acquisition, another 9.016-s cycle
353 restarted, and sixteen traces were averaged automatically to improve the signal-to-noise ratio. The
354 photochemical yield of PSI, ϕ_I, was calculated as $(P_M'-P)/P_M$; the non-photochemical yield of the PSI acceptor
355 side, ϕ_{NA}, was calculated as $(P_M-P_M')/P_M$; the non-photochemical yield of PSI due to the donor side limitation,
356 ϕ_{ND}, was calculated as P/P_M. The rate of P700 re-reduction was obtained from the initial slope of $P700^+$ decline
357 in the dark.

358 **Leaf spectroscopic and fluorescence analyses**

359 Leaf PSII and PSI yields were measured with the Dual PAM-100 (Heinz Walz) under the red actinic light (635
360 nm). PSII activity was assessed with the pulse amplitude modulated fluorescence method using 620 nm
361 measuring light of 9 µmol m^{-2} s^{-1}. The redox state of P700 was assessed by detecting absorbance changes of
362 the cation at 830 nm with a dual wavelength unit (830/875 nm). Saturating pulses of red light (635 nm) at
363 12,000 µmol m^{-2} s^{-1} were used. Leaves were first dark adapted for 30 min and then the maximum (F_M) and the
364 minimum (F_0) levels of fluorescence in the dark were recorded upon the application of a saturating pulse. The
365 maximum quantum yield of PSII (F_V/F_M) was calculated from those values as $(F_M- F_0)/ F_M$. Then, the maximal
366 $P700^+$ signal (P_M) was recorded upon the application of a saturating pulse at the end of the far-red light (720
367 nm) illumination, and the minimal $P700^+$ signal (P_0) was recorded after the saturating pulse. After that, leaves
368 were illuminated for 10 min with actinic light of 400 µmol m^{-2} s^{-1} followed by 2 min of darkness, during which
369 saturating pulses were applied every 40 s to probe for a build-up and relaxation of NPQ. NPQ was calculated
370 after Bilger and Björkman [67] as $(F_M-F_M')/F_M'$ where F_M' is the maximum level of fluorescence under light
371 recorded upon the application of a saturating pulse.

372 PSI and PSII parameters were then tested at 2-min intervals of increasing irradiance (0 to 1890 µmol m^{-2} s^{-1}) by
373 applying a saturating pulse at the end of each period. Recording F_M' and F (the fluorescence level briefly before
374 the application of a saturating pulse) allowed tracking of the partitioning of absorbed excitation energy within
375 PSII between the photochemical (ϕ_{II}) and non-photochemical reactions, including the regulated (ϕ_{NPQ}) and
376 non-regulated (ϕ_{NO}) fractions[68]. Using the steady-state $P700^+$ signal (P) and the maximal $P700^+$ signal under
377 light (P_M') recorded just before and upon the pulse application, respectively, we calculated the photochemical
378 yield of PSI (ϕ_I) and the non-photochemical yields of PSI due the acceptor (ϕ_{NA}) or donor (ϕ_{ND}) side limitations[69].

379 **Gas-exchange analysis**

380 Concomitant gas exchange and fluorescence analyses were performed at different irradiances and intercellular
381 CO_2 partial pressures using a LI-6800 (LI-COR Biosciences, Lincoln, NE, USA) equipped with a fluorometer head
382 6800-01A (LI-COR Biosciences). 90% red/10% blue actinic light was used for all measurements. First, leaves
383 were equilibrated at 381 µbar CO_2 in the reference side, leaf temperature 25°C, 60% humidity, and a flow rate
384 of 500 µmol s^{-1}. Then, either CO_2 partial pressures from 0 to 1200 µbar were imposed at 3-min intervals at a
385 constant irradiance of 1500 µmol m^{-2} s^{-1} (CO_2 response curve) or a stepwise increase of irradiance from 0 to
386 2000 µmol m^{-2} s^{-1} at 2-min intervals was imposed at a constant 381 µbar of CO_2 in the reference side (light
387 response curve). A relative electron flux through PSII (i x ϕ_{II}) was estimated upon the application of multiphase
388 saturating pulses (8000 µmol m^{-2} s^{-1}) as irradiance multiplied by the photochemical yield of PSII[70].

389 **Thylakoid membrane energisation**

390 Electrochromic shift signal (ECS) was monitored as absorbance changes between 550 and 515 nm with the
391 Dual PAM-100 equipped with the P515/535 emitter-detector module (Heinz Walz) and normalised for the
392 amplitude of ECS response to a saturating pulse (20 ms, 14,000 µmol m^{-2} s^{-1}) measured from the dark-adapted
393 leaves. Measurements were conducted on dark-adapted for 40 min leaves during 3-min light and 3-min dark
394 intervals of increasing irradiance. Proton motive force (*pmf*) and ΔpH were estimated upon the shift from light
395 to dark (Fig. S4)[71]. Proton conductivity of the thylakoid membrane (g_{H+}) was calculated as an inverse time
396 constant of the first order exponential ECS decay[70] fitted in OriginPro 2018b (OriginLab, Northampton, MA,
397 USA), and the light-driven proton flux (ν_{H+}) was calculated as the initial rate of change in the ECS signal upon
398 light termination[72].

399 **Statistical analysis**

400 ANOVA and two-tailed heteroscedastic Student's *t*-test were performed in OriginPro 2018b. Details of
401 replication, *post-hoc* tests and *P* values are provided in the main text and in figure legends.

402 **Acknowledgements**

403 We thank Brendon Conlan and Spencer Whitney for a gift of vectors and antibodies, Fred Chow for equipment
404 and assistance with P700 measurements, Xueqin Wang for Setaria transformation, and Emily Watson, Samuel
405 James Nix and Zac Taylor for technical assistance. This work was supported by the Australian Research Council
406 Centre of Excellence for Translational Photosynthesis (CE140100015).

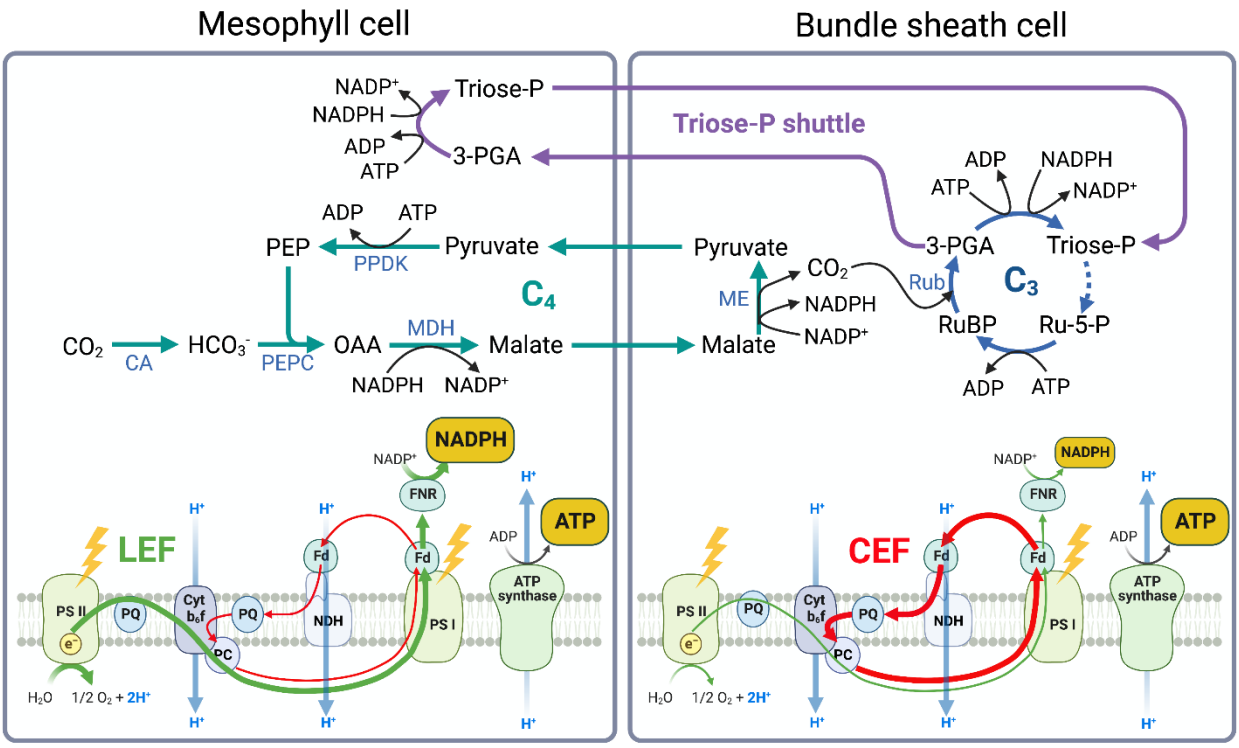

Fig. 1. Schematic representation of metabolic (top part) and light (bottom part) reactions of C_4 photosynthesis. CA, carbonic anhydrase; PEP, phosphoenolpyruvate; PEPC, phosphoenolpyruvate carboxylase; PPDK, pyruvate phosphate dikinase; OAA, oxaloacetate; MDH, malate dehydrogenase; ME, $NADP^+$-dependent malic enzyme; RuBP, ribulose-5-bisphosphaste; Rub, Rubisco; 3-PGA, 3-phospho-glyceraldehyde; Triose-P, triose phosphate; Ru-5-P, ribulose-5-phosphate; LEF, linear electron flow; CEF, cyclic electron flow; PSII, Photosystem II; PQ, plastoquinone; $Cytb_6f$, Cytochrome b_6f complex; PC, plastocyanin; NDH, chloroplast NADH dehydrogenase-like complex; Fd, ferredoxin; PSI, Photosystem I; FNR, ferredoxin:$NADP^+$ oxidoreductase.

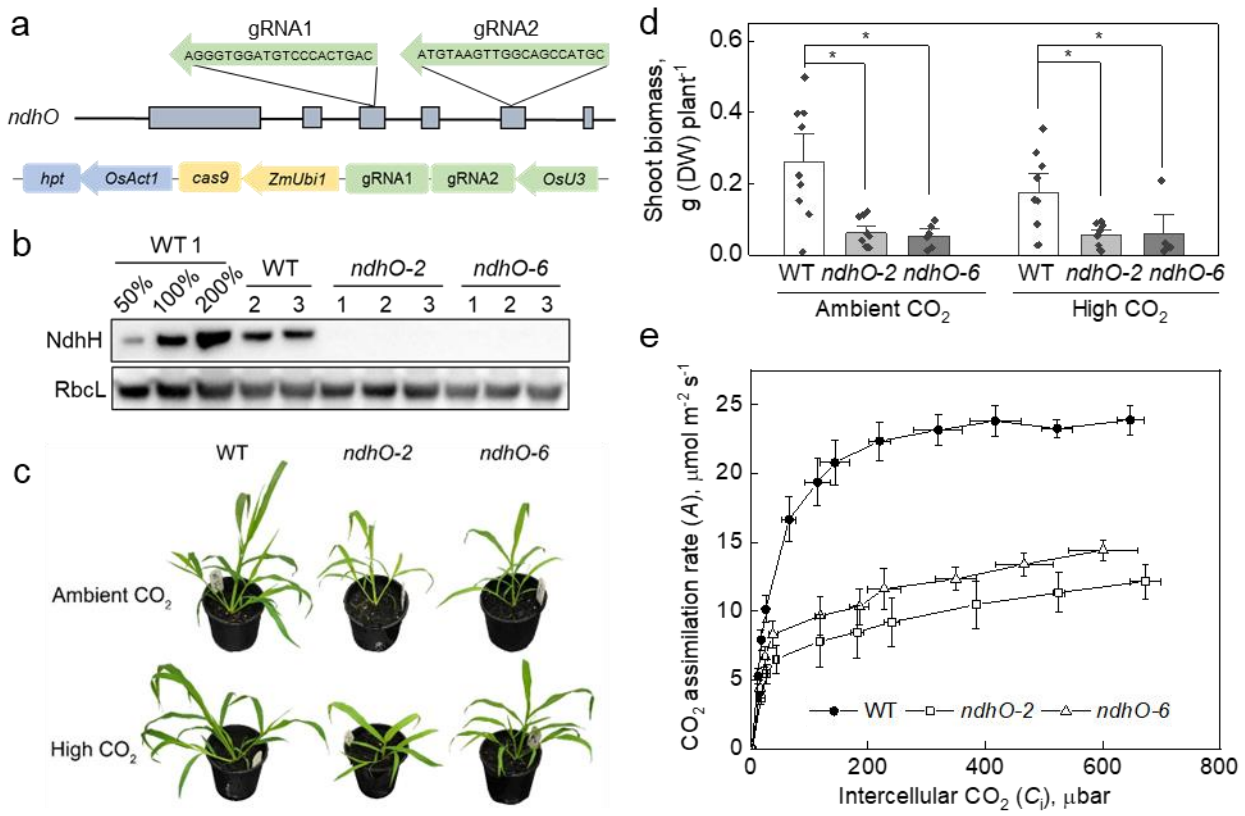

Fig. 2. Creating *S. viridis* plants lacking NDH complex. **a**. Positions of guide RNAs (gRNAs) within the third and fifth exons of the *ndhO* genomic sequence and schematics of the gene construct assembled for transformation (see details in Materials and Methods). **b**. Immunodetection of the NdhH subunit of NDH and the large subunit of Rubisco (RbcL) in leaf protein extracts from wild-type (WT) and *ndhO-2* and *ndhO-6* plants with homozygous null *ndhO* alleles loaded on leaf area basis. Relative quantification of the blots is shown in Fig. S2. (**c**, **d**) Phenotype and biomass of plants grown for two weeks in air (Ambient CO_2) or in air with 2% CO_2 (High CO_2). **d**. Mean ± SE, points are biological replicates. Asterisks indicate significant differences between edited and WT plants (P = 0.00003 for *ndhO-2*, P = 0.0002 for *ndhO-6*), no differences were found between *ndhO-2* and *ndhO-6* plants (P = 0.99) or between the CO_2 treatments (P = 0.24) using two-way ANOVA and Tukey's *post-hoc* test at $\alpha = 0.05$. **e**. Response of CO_2 assimilation rate (A) to intercellular CO_2 partial pressures (C_i) measured at 1500 µmol photons m^{-2} s^{-1} from plants grown at ambient CO_2. Mean ± SE, n = 5 biological replicates. A was significantly decreased in both *ndhO-2* and *ndhO-6* plants compared to WT at C_i above 100 µbar (one-way ANOVA and Tukey's *post-hoc* test at $\alpha = 0.05$).

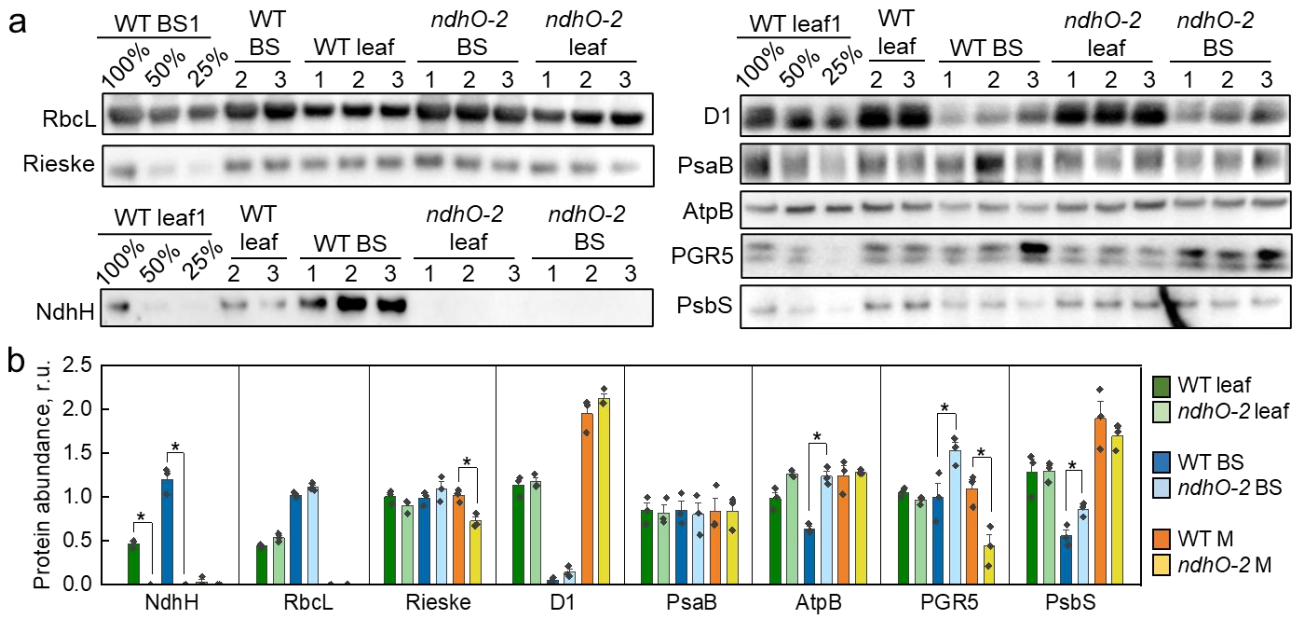

Fig. 3. Abundance of photosynthetic proteins in wild type (WT) *S. viridis* and *ndhO-2* plants lacking NDH. **a**. Immunodetection of RbcL (the large subunit of Rubisco), Rieske (Cytb_6f), NdhH (NDH), D1 (PSII), PsaB (PSI), AtpB (ATP synthase), PGR5 (the lower band, see Fig S6 for details) and PsbS in bundle sheath (BS) or leaf protein samples loaded on Chl (*a* + *b*) basis. Three biological replicates (1, 2, 3) were loaded for each group and the titration series of one of the samples was used for relative quantification. **b**. Relative quantification of protein abundance per unit of Chl in leaves, BS and mesophyll (M) cells. Mean ± SE and three replicates are shown. Each protein has its own relative scale. Asterisks indicate statistically significant differences between the same cell types of WT and *ndhO-2* plants (*t*-test, $P < 0.05$).

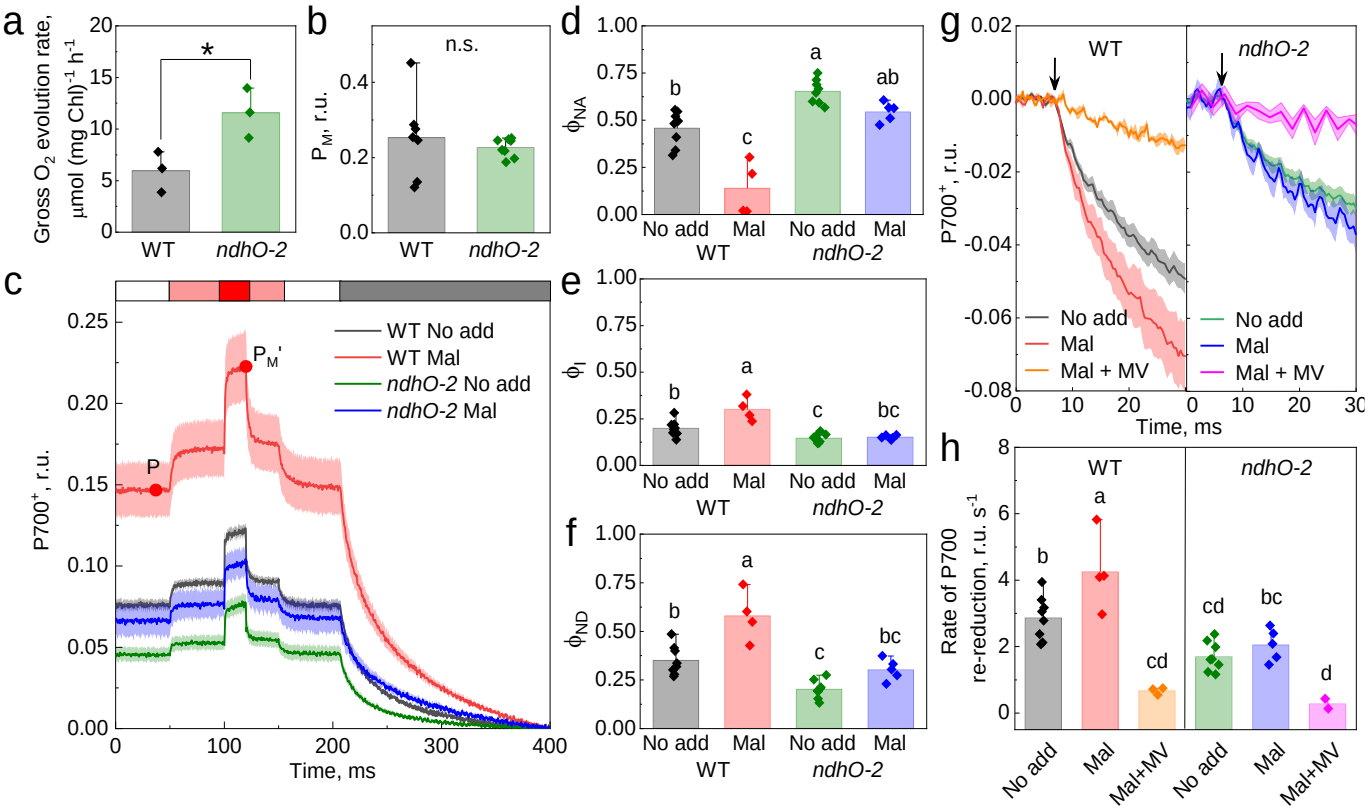

Fig. 4. Photosynthetic properties of bundle sheath (BS) strands isolated from leaves of wild-type (WT) *S. viridis* and *ndhO-2* plants lacking NDH complex. All BS preparations were normalised to 25 µg Chl mL^{-1} and supplemented with $NaHCO_3$ and triose phosphate. **a**. Gross O_2 evolution rates of BS strands illuminated with white actinic light of 1000 µmol m^{-2} s^{-1} (*t*-test at $P < 0.05$). **b**. The maximum photo-oxidisable P700 (PSI reaction centre), P_M (n.s., not significant; *t*-test at $P < 0.05$). **c.** Fast kinetics of $P700^+$ signal recorded from BS strands with or without 10 mM malate. BS were illuminated with white actinic light of 1000 µmol m^{-2} s^{-1} (white bar on top of the graph), actinic light with added far-red light (pink bar) or combined actinic, far-red light and a saturating pulse (red bar). Points on the WT trace with malate demonstrate how the P (the steady-state P700 oxidation level) and P_M' (the maximum level of P700 oxidation under light) values were obtained. **d.** The non-photochemical yield of PSI due to the acceptor side limitation (ϕ_{NA}) calculated as $(P_M-P_M')/P_M$. **e**. The effective quantum yield of PSI (ϕ_I) calculated as $(P_M'-P)/P_M$. **f.** The non-photochemical yield of PSI due to the donor side limitation (ϕ_{ND}) calculated as P/P_M. **g**. Fast kinetics of $P700^+$ signal upon the light-dark shift normalised for the steady-state $P700^+$ level for comparison of the kinetics. Arrows indicate the end of illumination. 200 µM of methyl viologen (MV) was added in addition to 10 mM of malate when indicated. **f**. The relative rate of P700 re-reduction estimated from initial slopes of the dark relaxation kinetics shown in (g). All bar graphs show Mean ± SD. (**c**, **g**) Traces are average of 2-5 biological replicates. Mean ± SE. (**d**, **e**, **f**, **h**) Letters indicate significant differences between the groups (one-way ANOVA and Tukey's *post-hoc* test at $\alpha > 0.05$).

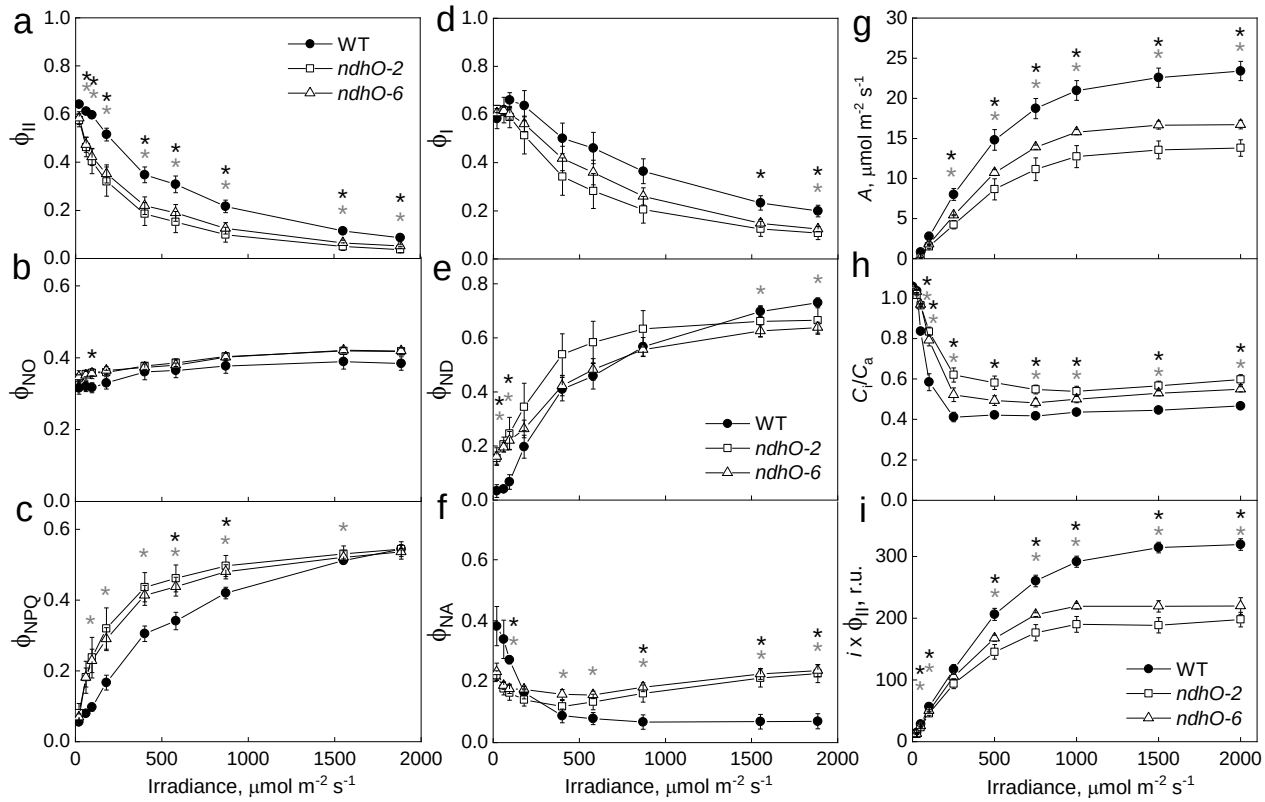

Fig. 5. Leaf photosynthesis in wild-type *S. viridis* (WT) and gene-edited plants lacking NDH (*ndhO-2* and *ndhO-6*). (**a**, **b**, **c**) The photochemical yield of PSII (ϕ_{II}), the yield of non-regulated energy dissipation (ϕ_{NO}) and the yield of non-photochemical quenching (ϕ_{NPQ}) in PSII. (**d**, **e**, **f**) The photochemical yield of PSI (ϕ_{I}) and the non-photochemical yields of PSI donor (ϕ_{ND}) and acceptor (ϕ_{NA}) sides. PSI and PSII quantum yields were analysed concomitantly at different irradiance with Dual-PAM-100. (**g**, **h**, **i**) CO_2 assimilation rate (*A*), the ratio of intercellular to ambient CO_2 partial pressures (C_i/C_a) and a relative electron flux through PSII (i x ϕ_{II}) measured concomitantly at different irradiance using Licor-6800. Mean ± SE, n = 4 biological replicates. Asterisks indicate statistically significant differences between the edited and WT plants (one-way ANOVA and Dunnett's *post-hoc* test, α = 0.05): black asterisks for *ndhO-2*, grey asterisks for *ndhO-6*.

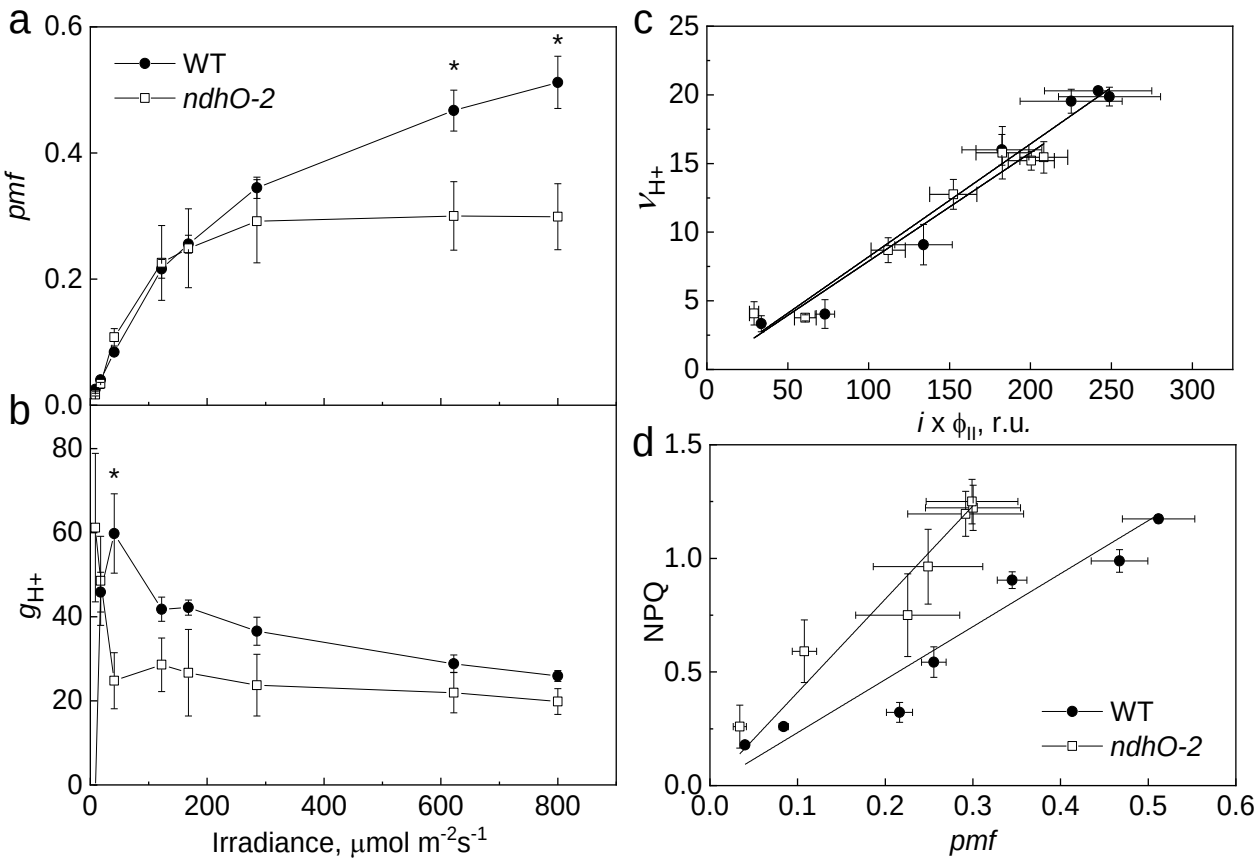

Fig. 6. Thylakoid membrane energisation in wild-type (WT) *S. viridis* and gene-edited plants lacking NDH (*ndhO-2*). (**a**, **b**) Proton motive force (*pmf*) and proton conductivity of the thylakoid membrane (g_{H+}) after 3-min illumination at different irradiance. **c**. The relationship between the light-driven proton flux (ν_{H+}) and the relative electron flux through PSII. The slope of linear regression of ν_{H+} versus i x ϕ_{II} is 0.088 ±0.017 for WT and 0.080 ±0.012 for *ndhO-2* (P = 0.71). **d**. The relationship between the energy-dependent non-photochemical quenching (NPQ) and *pmf*. The slope of linear regression of NPQ versus *pmf* is 2.25 ±0.6 for WT and 4.14 ±0.33 for *ndhO-2* (P = 0.03). Mean ± SE, n = 4 biological replicates. Asterisks indicate statistically significant differences between the edited and WT plants at $P < 0.05$. The relationship between mean values of edited and WT plants was tested by the Student's *t*-test.

481 **References**

482 1 Sage, R. F. & Zhu, X.-G. Exploiting the engine of C_4 photosynthesis. *Journal of Experimental Botany* **62**,
483 2989-3000 (2011).
484 2 Long, S. P. Environmental responses. *C_4 plant biology*, 215-249 (1999).
485 3 Hatch, M. D. C_4 photosynthesis - a unique blend of modified biochemistry, anatomy and ultrastructure.
486 *Biochimica Et Biophysica Acta* **895**, 81-106 (1987).
487 4 Furbank, R. T. Evolution of the C_4 photosynthetic mechanism: are there really three C_4 acid
488 decarboxylation types? *Journal of Experimental Botany* **62**, 3103-3108 (2011).
489 https://doi.org:10.1093/jxb/err080
490 5 Ermakova, M. *et al.* Installation of C_4 photosynthetic pathway enzymes in rice using a single construct.
491 *Plant Biotechnology Journal* **19**, 575-588 (2021).
492 6 Ermakova, M., Danila, F. R., Furbank, R. T. & von Caemmerer, S. On the road to C_4 rice: advances and
493 perspectives. *The Plant Journal* **101**, 940-950 (2020).
494 7 Munekage, Y. Light harvesting and chloroplast electron transport in NADP-malic enzyme type C_4 plants.
495 *Current Opinion in Plant Biology* **31**, 9-15 (2016).
496 8 Malone, L. A., Proctor, M. S., Hitchcock, A., Hunter, C. N. & Johnson, M. P. Cytochrome b6f –
497 orchestrator of photosynthetic electron transfer. *Biochimica et Biophysica Acta (BBA) - Bioenergetics*
498 **1862**, 148380 (2021). https://doi.org:https://doi.org/10.1016/j.bbabio.2021.148380
499 9 Müller, P., Li, X.-P. & Niyogi, K. K. Non-photochemical quenching. A response to excess light energy.
500 *Plant physiology* **125**, 1558-1566 (2001).
501 10 Li, X.-P. *et al.* Regulation of photosynthetic light harvesting involves intrathylakoid lumen pH sensing
502 by the PsbS protein. *Journal of Biological Chemistry* **279**, 22866-22874 (2004).
503 11 Demmig-Adams, B. Carotenoids and photoprotection in plants: A role for the xanthophyll zeaxanthin.
504 *Biochimica et Biophysica Acta (BBA) - Bioenergetics* **1020**, 1-24 (1990).
505 12 Kramer, D. M. & Evans, J. R. The importance of energy balance in improving photosynthetic
506 productivity. *Plant Physiology* **155**, 70-78 (2011).
507 13 von Caemmerer, S. & Furbank, R. T. Strategies for improving C_4 photosynthesis. *Current Opinion in*
508 *Plant Biology* **31**, 125-134 (2016).
509 14 Ermakova, M. *et al.* Upregulation of bundle sheath electron transport capacity under limiting light in
510 C_4 *Setaria viridis*. *The Plant Journal* **106**, 1443-1454 (2021).
511 15 Furbank, R., Jenkins, C. & Hatch, M. C_4 photosynthesis: quantum requirement, C_4 and overcycling and
512 Q-cycle involvement. *Functional Plant Biology* **17**, 1-7 (1990).
513 16 Woo, K. C., Gerbaud, A. & Furbank, R. T. Evidence for endogenous cyclic photophosphorylation in intact
514 chloroplasts: $^{14}CO_2$ fixation with dihydroxyacetone phosphate. *Plant Physiology* **72**, 321-325 (1983).
515 17 Shikanai, T. Cyclic Electron Transport Around Photosystem I: Genetic Approaches. *Annual Review of*
516 *Plant Biology* **58**, 199-217 (2007). https://doi.org:10.1146/annurev.arplant.58.091406.110525
517 18 Munekage, Y. *et al.* Elevated expression of PGR5 and NDH-H in bundle sheath chloroplasts in C_4 *Flaveria*
518 species. *Plant and Cell Physiology* **51**, 664-668 (2010).
519 19 Munekage, Y. & Taniguchi, Y. Y. Promotion of cyclic electron transport around Photosystem I with the
520 development of C_4 photosynthesis. *Plant and Cell Physiology* **57**, 897-903 (2016).
521 20 Majeran, W. *et al.* Consequences of C_4 differentiation for chloroplast membrane proteomes in maize
522 mesophyll and bundle sheath cells. *Molecular & Cellular Proteomics* **7**, 1609-1638 (2008).
523 21 Kubicki, A., Funk, E., Westhoff, P. & Steinmüller, K. Differential expression of plastome-encoded *ndh*
524 genes in mesophyll and bundle-sheath chloroplasts of the C_4 plant *Sorghum bicolor* indicates that the
525 complex I-homologous NAD(P)H-plastoquinone oxidoreductase is involved in cyclic electron transport.
526 *Planta* **199**, 276-281 (1996).
527 22 Takabayashi, A., Kishine, M., Asada, K., Endo, T. & Sato, F. Differential use of two cyclic electron flows
528 around photosystem I for driving CO_2-concentration mechanism in C_4 photosynthesis. *Proceedings of*
529 *the National Academy of Sciences of the United States of America* **102**, 16898-16903 (2005).
530 23 Sazanov, L. A., Burrows, P. & Nixon, P. J. Detection and characterization of a complex I-like NADH-
531 specific dehydrogenase from pea thylakoids. *Biochemical Society Transactions* **24**, 739-743 (1996).
532 24 Shikanai, T. *et al.* Directed disruption of the tobacco *ndhB* gene impairs cyclic electron flow around
533 photosystem I. *Proceedings of the National Academy of Sciences* **95**, 9705-9709 (1998).

25 Peterson, R. B., Schultes, N. P., McHale, N. A. & Zelitch, I. Evidence for a role for NAD(P)H dehydrogenase in concentration of CO_2 in the bundle sheath cell of *Zea mays*. *Plant Physiology* **171**, 125 (2016).

26 Ishikawa, N. *et al.* NDH-mediated cyclic electron flow around Photosystem I is crucial for C_4 photosynthesis. *Plant and Cell Physiology* **57**, 2020-2028 (2016).

27 Ogawa, T. *et al.* Two cyclic electron flows around photosystem I differentially participate in C_4 photosynthesis. *Plant Physiology* (2023). https://doi.org:10.1093/plphys/kiad032

28 Alonso-Cantabrana, H. *et al.* Diffusion of CO_2 across the mesophyll-bundle sheath cell interface in a C_4 plant with genetically reduced PEP carboxylase activity. *Plant Physiology* **178**, 72-81 (2018).

29 Danila, F. R. *et al.* Bundle sheath suberisation is required for C_4 photosynthesis in a *Setaria viridis* mutant. *Communications Biology* **4**, 254 (2021).

30 Furbank, R. T. & Badger, M. R. Photorespiratory characteristics of isolated bundle sheath strands of C_4 monocotyledons. *Functional Plant Biology* **10**, 451-458 (1983).

31 Baker, N. R., Harbinson, J. & Kramer, D. M. Determining the limitations and regulation of photosynthetic energy transduction in leaves. *Plant, Cell & Environment* **30**, 1107-1125 (2007). https://doi.org:doi:10.1111/j.1365-3040.2007.01680.x

32 Laughlin, T. G., Savage, D. F. & Davies, K. M. Recent advances on the structure and function of NDH-1: The complex I of oxygenic photosynthesis. *Biochimica et Biophysica Acta (BBA) - Bioenergetics* **1861**, 148254 (2020).

33 Ruhlman, T. A. *et al.* NDH expression marks major transitions in plant evolution and reveals coordinate intracellular gene loss. *BMC Plant Biology* **15**, 100 (2015).

34 Strand, D. D., Fisher, N. & Kramer, D. M. The higher plant plastid NAD(P)H dehydrogenase-like complex (NDH) is a high efficiency proton pump that increases ATP production by cyclic electron flow. *Journal of Biological Chemistry* **292**, 11850-11860 (2017).

35 Livingston, A. K., Cruz, J. A., Kohzuma, K., Dhingra, A. & Kramer, D. M. An Arabidopsis mutant with high cyclic electron flow around Photosystem I (*hcef*) Involving the NADPH dehydrogenase complex *The Plant Cell* **22**, 221-233 (2010).

36 Yamori, W., Makino, A. & Shikanai, T. A physiological role of cyclic electron transport around photosystem I in sustaining photosynthesis under fluctuating light in rice. *Scientific Reports* **6** (2016). https://doi.org:10.1038/srep20147

37 Nakano, H., Yamamoto, H. & Shikanai, T. Contribution of NDH-dependent cyclic electron transport around photosystem I to the generation of proton motive force in the weak mutant allele of *pgr5*. *Biochimica et Biophysica Acta (BBA) - Bioenergetics* **1860**, 369-374 (2019). https://doi.org:https://doi.org/10.1016/j.bbabio.2019.03.003

38 Lyu, M.-J. A. *et al.* The coordination of major events in C_4 photosynthesis evolution in the genus *Flaveria*. *Scientific Reports* **11**, 15618 (2021).

39 von Caemmerer, S. Updating the steady state model of C_4 photosynthesis. *Journal of Experimental Botany* **72**, 6003-6017 (2021). https://doi.org:10.1101/2021.03.13.435281

40 Sagun, J. V., Badger, M. R., Chow, W. S. & Ghannoum, O. Cyclic electron flow and light partitioning between the two photosystems in leaves of plants with different functional types. *Photosynthesis Research* **142**, 321-334 (2019). https://doi.org:10.1007/s11120-019-00666-1

41 Bellasio, C. & Ermakova, M. Reduction of bundle sheath size boosts cyclic electron flow in C_4 *Setaria viridis* acclimated to low light. *The Plant Journal* **111**, 1223-1237 (2022).

42 Kanazawa, A. *et al.* Chloroplast ATP synthase modulation of the thylakoid proton motive force: implications for Photosystem I and Photosystem II photoprotection. *Frontiers in Plant Science* **8** (2017). https://doi.org:10.3389/fpls.2017.00719

43 Tazoe, Y. *et al.* Overproduction of PGR5 enhances the electron sink downstream of Photosystem I in a C_4 plant, *Flaveria bidentis*. *The Plant Journal* **103**, 814-823 (2020).

44 Peltier, G., Aro, E.-M. & Shikanai, T. NDH-1 and NDH-2 plastoquinone reductases in oxygenic photosynthesis. *Annual Review of Plant Biology* **67**, 55-80 (2016). https://doi.org:10.1146/annurev-arplant-043014-114752

45 Osmond, B. Carbon reduction and photosystem II deficiency in leaves of C_4 plants. *Aust J Plant Physiol*, 41-50 (1974).

587 46 Ivanov, B., Asada, K., Kramer, D. M. & Edwards, G. Characterization of photosynthetic electron
588 transport in bundle sheath cells of maize. I. Ascorbate effectively stimulates cyclic electron flow around
589 PSI. *Planta* **220**, 572-581 (2005).
590 47 Bellasio, C. & Lundgren, M. R. Anatomical constraints to C_4 evolution: light harvesting capacity in the
591 bundle sheath. *New Phytologist* **212**, 485–496 (2016).
592 48 Ehleringer, J. & Pearcy, R. W. Variation in Quantum Yield for CO2 Uptake among C3 and C4 Plants.
593 *Plant Physiology* **73**, 555-559 (1983). https://doi.org:Doi 10.1104/Pp.73.3.555
594 49 Munekage, Y. *et al.* PGR5 is involved in cyclic electron flow around Photosystem I and is essential for
595 photoprotection in Arabidopsis. *Cell* **110**, 361-371 (2002).
596 50 Siebke, K., von Caemmerer, S., Badger, M. & Furbank, R. T. Expressing an *rbcS* antisense gene in
597 transgenic *Flaveria bidentis* leads to an increased quantum requirement for CO_2 fixed in Photosystems
598 I and II. *Plant Physiology* **115**, 1163-1174 (1997).
599 51 Ermakova, M., Lopez-Calcagno, P. E., Raines, C. A., Furbank, R. T. & von Caemmerer, S. Overexpression
600 of the Rieske FeS protein of the Cytochrome b_6f complex increases C_4 photosynthesis in *Setaria viridis*.
601 *Communications Biology* **2** (2019).
602 52 Nikkanen, L., Guinea Diaz, M., Toivola, J., Tiwari, A. & Rintamäki, E. Multilevel regulation of non-
603 photochemical quenching and state transitions by chloroplast NADPH-dependent thioredoxin
604 reductase. *Physiologia Plantarum* **166**, 211-225 (2019).
605 https://doi.org:https://doi.org/10.1111/ppl.12914
606 53 Da, Q. *et al.* M-type thioredoxins are involved in the xanthophyll cycle and proton motive force to alter
607 NPQ under low-light conditions in Arabidopsis. *Plant Cell Reports* **37**, 279-291 (2018).
608 https://doi.org:10.1007/s00299-017-2229-6
609 54 Concordet, J.-P. & Haeussler, M. CRISPOR: intuitive guide selection for CRISPR/Cas9 genome editing
610 experiments and screens. *Nucleic Acids Research* **46**, 242-245 (2018).
611 55 Hassan, M. M. *et al.* Construct design for CRISPR/Cas-based genome editing in plants. *Trends in Plant*
612 *Science* **26**, 1133-1152 (2021).
613 56 Xie, K., Minkenberg, B. & Yang, Y. Boosting CRISPR/Cas9 multiplex editing capability with the
614 endogenous tRNA-processing system. *Proceedings of the National Academy of Sciences* **112**, 3570-
615 3575 (2015).
616 57 Engler, C. *et al.* A Golden Gate modular cloning toolbox for plants. *ACS Synthetic Biology* **3**, 839-843
617 (2014).
618 58 Osborn, H. L. *et al.* Effects of reduced carbonic anhydrase activity on CO_2 assimilation rates in *Setaria*
619 *viridis*: a transgenic analysis. *Journal of Experimental Botany* **68**, 299-310 (2016).
620 59 Jumper, J. *et al.* Highly accurate protein structure prediction with AlphaFold. *Nature* **596**, 583-589
621 (2021).
622 60 Sehnal, D. *et al.* Mol* Viewer: modern web app for 3D visualization and analysis of large biomolecular
623 structures. *Nucleic Acids Research* **49**, 431-437 (2021).
624 61 Porra, R. J., Thompson, W. A. & Kriedemann, P. E. Determination of accurate extinction coefficients
625 and simultaneous equations for assaying chlorophylls a and b extracted with four different solvents:
626 verification of the concentration of chlorophyll standards by atomic absorption spectroscopy.
627 *Biochimica et Biophysica Acta (BBA) - Bioenergetics* **975**, 384-394 (1989).
628 62 Ghannoum, O. *et al.* Faster rubisco is the key to superior nitrogen-use efficiency in NADP-malic enzyme
629 relative to NAD-malic enzyme C_4 grasses. *Plant Physiology* **137**, 638-650 (2005).
630 63 Martin-Avila, E. *et al.* Modifying plant photosynthesis and growth via simultaneous chloroplast
631 transformation of Rubisco large and small subunits. *The Plant Cell* **32**, 2898-2916 (2020).
632 64 Karki, S. *et al.* A role for neutral variation in the evolution of C_4 photosynthesis. *bioRxiv* (2020).
633 https://doi.org:10.1101/2020.05.19.104299
634 65 Beckmann, K., Messinger, J., Badger, M. R., Wydrzynski, T. & Hillier, W. On-line mass spectrometry:
635 membrane inlet sampling. *Photosynthesis research* **102**, 511-522 (2009).
636 66 Kou, J. *et al.* Estimation of the steady-state cyclic electron flux around PSI in spinach leaf discs in white
637 light, CO_2-enriched air and other varied conditions. *Functional Plant Biology* **40**, 1018-1028 (2013).
638 67 Bilger, W. & Björkman, O. Role of the xanthophyll cycle in photoprotection elucidated by
639 measurements of light-induced absorbance changes, fluorescence and photosynthesis in leaves of
640 *Hedera canariensis*. *Photosynthesis Research* **25**, 173-185 (1990).

641 68 Kramer, D., Johnson, G., Kiirats, O. & Edwards, G. New fluorescence parameters for the determination
642 of QA redox state and excitation energy fluxes. *Photosynthesis Research* **79**, 209-218 (2004).
643 69 Klughammer, C. & Schreiber, U. Saturation pulse method for assessment of energy conversion in PS I.
644 *PAM Application notes* **1**, 3 (2008).
645 70 Sacksteder, C. A., Kanazawa, A., Jacoby, M. E. & Kramer, D. M. The proton to electron stoichiometry of
646 steady-state photosynthesis in living plants: a proton-pumping Q cycle is continuously engaged.
647 *Proceedings of the National Academy of Sciences* **97**, 14283-14288 (2000).
648 71 Takizawa, K., Cruz, J. A., Kanazawa, A. & Kramer, D. M. The thylakoid proton motive force in vivo.
649 Quantitative, non-invasive probes, energetics, and regulatory consequences of light-induced pmf.
650 *Biochimica et Biophysica Acta (BBA) - Bioenergetics* **1767**, 1233-1244 (2007).
651 72 Takizawa, K., Kanazawa, A. & Kramer, D. M. Depletion of stromal Pi induces high 'energy-dependent'
652 antenna exciton quenching (qE) by decreasing proton conductivity at CFO-CF1 ATP synthase. *Plant,*
653 *Cell & Environment* **31**, 235-243 (2008).

654